JACS
JOURNAL OF THE AMERICAN CHEMICAL SOCIETY
Article
pubs.acs.org/JACS

First-Principles Study of Phenol Hydrogenation on Pt and Ni Catalysts in Aqueous Phase

Yeohoon Yoon,[†] Roger Rousseau,*[,†] Robert S. Weber,[†] Donghai Mei,*[,†] and Johannes A. Lercher*[,†,‡]

[†]Institute for Integrated Catalysis, Pacific Northwest National Laboratory, Richland, Washington 99352, United States
[‡]Department of Chemistry and Catalysis Research Institute, Technische Universität München, Garching 85747, Germany

Supporting Information

ABSTRACT: The effect of an aqueous phase on phenol hydrogenation over Pt and Ni catalysts was investigated using density functional theory-based ab initio molecular dynamics calculations. The adsorption of phenol and the addition of the first and second hydrogen adatoms to three, ring carbon positions (*ortho*, *meta*, and *para* with respect to the phenolic OH group) were explored in both vacuum and liquid water. The major change in the electronic structure of both Pt(111) and Ni(111) surfaces, between a gaseous and liquid phase environment, results from a repulsion between the electrons of the liquid water and the diffuse tail of electron density emanating from the metal surface. The redistribution of the metal's electrons toward the subsurface layer lowers the metal work function by about 1 eV. The lower work function gives the liquid-covered metal a higher chemical reduction strength and, in consequence, a lower oxidation strength, which, in turn lowers the phenol adsorption energy, despite the stabilizing influence of the solvation of the partly positively charged adsorbate. At both the solid/vapor and the solid/water interface, H adatom addition involves neutral H atom transfer hence the reaction barriers for adding H adatoms to phenol are lowered by only 10−20 kJ/mol, due to a small stabilizing at the transition state. More importantly, the liquid environment significantly influences the relative energetics of charged, surface-bound intermediates and of proton-transfer reactions like keto/enol isomerization. For phenol hydrogenation, solvation in water results in an energetic preference to form ketones as a result of tautomerization of surface-bound enol intermediates.

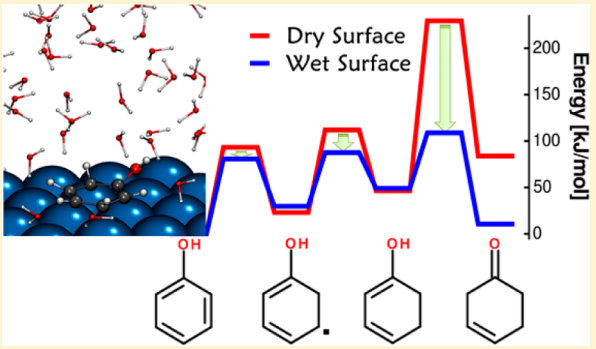

1. INTRODUCTION

Catalytic upgrading of bio-oils is an important step in the production of transportation fuels from biomass-derived resources.[1−9] The bio-oils generated by fast pyrolysis or liquefaction generally contain oxygenates such as carboxylic acids, aldehydes, ketones, alcohols, and especially a substantial concentration of phenolic compounds.[10,11] To increase the energy density and the stability of bio-oils, hydrodeoxygenation (HDO) is used.[10,11] Since the HDO of bio-oils proceeds in the presence of substantial concentrations of water or in aqueous phase, industrial hydrotreating catalysts such as those derived from sulfided CoMo and NiMo are challenged due to leaching of sulfur and deactivation.[10,11] The low sulfur content of the biomass-derived bio-oils also discourages using sulfided catalysts, because they would need the addition of sulfur, at least periodically, during the HDO process. Therefore, effective, sulfur-free catalysis is needed for efficient biomass utilization as an energy carrier. The hydro-upgrading of phenol, the simplest phenolic compound, over supported metal catalysts has been discussed in detail.[4,9,12−14] Currently, it is believed that phenol is first hydrogenated into cyclohexanone and subsequently cyclohexanol over zeolite-supported metallic (Pd and Ni) catalysts (see Scheme 1). For phenol hydrogenation in aqueous phase on catalysts containing small particles of Pd and Ni,

Scheme 1. Phenol Hydrogenation Pathways Discussed in the Literature[a]

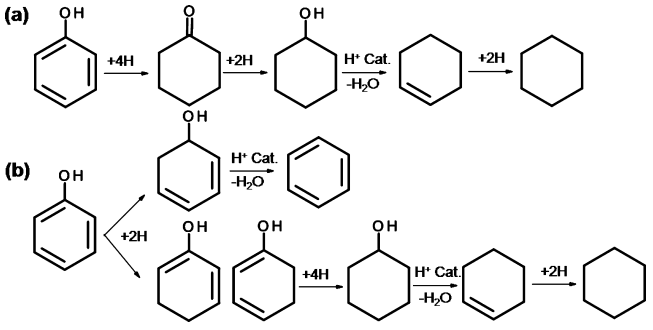

[a](a) Liquid phase (upper route) and (b) vapor phase (lower route).

cyclohexanone and cyclohexanol are the two, major products, and experimental evidence suggests that the reaction proceeds sequentially, selectively producing cyclohexanone first, which is further hydrogenated to cyclohexanol. Cyclohexanol is then dehydrated into cyclohexene over acid sites followed by

Received: February 14, 2014
Published: July 2, 2014

dx.doi.org/10.1021/ja501592y | J. Am. Chem. Soc. 2014, 136, 10287−10298

hydrogenation to cyclohexane. The selectivity toward cyclohexanone and cyclohexanol can be controlled, to some extent, using different additives and support materials, and by varying the H_2 pressure or the availability of hydrogen from reducing agents.[4,9,12,13]

Although extensive, experimental studies of phenol HDO in both vapor and aqueous phase have been carried out, very few studies on the reaction mechanisms and kinetics of phenol hydrogenation using surface-science techniques and detailed kinetic analysis have been reported. On the basis of the detailed analysis of products and electronic structure calculations, Mossoth et al. suggested that phenol hydrogenation on a sulfided CoMo catalyst proceeds via two parallel reaction pathways.[14] The first pathway leads to the formation of benzene and water (hydrogenolysis), while the second pathway catalyzes the formation of cyclohexene and cyclohexane via the cyclohexanol intermediate. This study proposed that the first hydrogenation step of phenol, i.e., hydrogenation of one of three C═C double bonds in the phenolic ring, determines which reaction pathways will be followed in the entire hydrogenation. The hydrogenation step, i.e., the addition of H_2, proceeds via two consecutive H adatom additions, in which surface-bound H adatoms are transferred to one of the carbon atoms on the adsorbed phenol. For these sulfided catalysts (at a solid/vapor interface), it is proposed that if the first hydrogen-addition step occurs at the *ortho* position of the phenolic ring, then C═O bond breaking is energetically favored and eventually the cyclohexene pathway dominates. On the other hand, if the first hydrogen-addition step occurs at the *meta* or the *para* position of the phenolic ring, the second reaction path leading to cyclohexanol will be favored (see Scheme 1). In this scenario, all three C═C bonds will be saturated before the C−O bond breaking, and cyclohexanol will be the preferred product.[14]

We note that this mechanistic alternative is very different from that described above for aqueous phase hydrogenation (both routes are represented in Scheme 1). The goal of the current paper is, therefore, to understand, if the presence of the solvent causes the difference. The current study examines the reaction energetics of the critical, first hydrogenation of surface-bound phenol on nonsulfided, base and precious metal catalysts using first-principles-based electronic structure methods. Here we will present a detailed atomic level understanding of how these reactions are influenced by the presence of water as well as by the nature of the hydrogenating metal.

First-principles density functional theory (DFT) calculations have been extensively used to study the interactions of reactants, intermediates and products to elucidate complex reaction mechanisms over metal catalysts.[15−18] Relatively few studies of phenol adsorption and reaction on metal surfaces have been reported.[19] Delle Site et al. found that phenol adsorbs on the Ni(111) surface in the parallel configuration with the hydroxyl group tilted away from the surface, while the vertical adsorption geometry is much less favored.[20,21] Honkala et al. recently studied the adsorption and dissociation of phenol on flat and stepped Pt and Rh surfaces.[22] They found that phenol adsorption on the stepped (211) surface is weaker than on a flat (111) surface. Although the calculated activation barriers of the O−H bond breaking on the Pt(111) and Rh(111) are calculated to be almost the same (66 and 63 kJ/mol respectively), phenol dehydrogenation to phenoxy is thermodynamically favorable (exothermic) on Rh(111), while it is unfavorable on the Pt(111) surface.

Molecular-level modeling of surface reactions in the presence of liquid solvent environments (aqueous or nonaqueous) is important for understanding both thermal and electrocatalytic processes for energy conversion and storage applications.[23−25] Due to the complexity of these interfacial phenomena and the dynamic nature of bulk and interfacial water adjacent to the metal surface, molecular level models of reactivity also require a high level of complexity. Such a model, in principle, can account for the solvation effects that stabilize reaction intermediates and transition states along the reaction pathways. However, this type of simulation is still extremely challenging and computationally demanding.[23−25]

We believe that an aqueous phase can possibly play two roles: it could modify the electronic structure of the metal catalyst surface; and the water molecules around the active surface site might directly participate in surface reactions by providing proton transfer and proton exchange pathways.[25,26] For example, acetic acid deprotonation on Pd(111) shifts from homolytic O−H bond breaking in the vapor phase to heterolytic dissociation in the presence of liquid water.[27] Desai and Neurock studied water dissociation over a PtRu alloy surface in the presence of 23 water molecules to represent the aqueous liquid phase environment.[28] That study found that water dissociation in the vapor/solid interface is strongly endothermic with a high barrier of 105 kJ/mol, whereas water dissociation at the solid/aqueous interface is less endothermic (+26 kJ/mol) with a much lower barrier of 27 kJ/mol. The possibility that the solvent may take part directly in the catalytic reactivity necessitates the technically challenging task of modeling catalysis at the solid/aqueous interface with an explicit representation of the solvating molecules.

In the present work, the effects of an aqueous phase on the hydrogenation of phenol over Pt and Ni catalysts were investigated using ab initio molecular dynamics (AIMD) calculations. First, the electronic structure and dynamical nature of H_2O/Pt(111) and H_2O/Ni(111) interfaces were studied with increasing water concentrations: vapor phase, monolayer and double layers of water, and finally using a model of the liquid bulk phase (explicitly described by 52 H_2O molecules). We have interpreted the AIMD results on the basis of a detailed analysis of the interfacial electrostatics induced by the addition of a liquid phase adjacent to the metal surface. We have studied phenol adsorption as well as the addition of the first and second H adatom at different carbon positions of the phenolic ring and demonstrate that for these metal surfaces the presence of the liquid phase strongly influences the selectivity toward production of cyclohexanone via facilitating keto/enol isomerization of surface-bound intermediates. As such, this work addresses the fundamental question of how an aqueous phase influences hydrogenation of aromatic rings on noble and base metal catalysts.

2. COMPUTATIONAL DETAILS

The calculations were carried out using the spin-polarized, gradient-corrected functional of Perdew, Burke, and Ernzerhof (PBE) as implemented in the CP2K package.[29] The wave functions were expanded in a molecularly optimized double-ζ Gaussian basis set to minimize basis set superposition errors.[30] An additional, auxiliary plane wave[31] basis of 320 Ry energy cutoff was used for the calculation of the electrostatic energy terms. Core electrons have been modeled by scalar relativistic norm-conserving pseudopotentials[32,33] with 1, 4, 6, and 18 valence electrons for H, C, O, and Ni/Pt, respectively. The Γ-point approximation was employed for Brillouin zone integration. The semiempirical van der Waals correction proposed by Grimme[34] has

been included in all calculations. The bulk metal Ni and Pt are represented by (111) bulk-terminated c(2 × 4) supercell slab models (16 surface atoms) of 4 atomic layers of thickness, for which we calculated work functions (W) of 4.9 and 5.6 eV for Ni and Pt respectively, which compare adequately with the experimental values of 5.3 (Ni)[35] and 5.8 eV (Pt).[36]

This representation of the metal surfaces allows for efficient and affordable AIMD simulations with a bulk liquid water phase containing 52 water molecules. The simulations were chosen to represent a high temperature (500 K) and pressure (4 MPa) conditions which are similar to that employed in aqueous phase hydrogenation experiments.[2−6,13,39,40] The simulation is first equilibrated in a constant pressure ensemble (NPT) for a duration of 2 ps to allow for the adjustment of the simulation cell axes to provide an isotropic stress across the entire system (both within the surface slab and between the slab and the liquid phase). In a second step, the simulations are equilibrated at T = 500 K in a canonical (NVT) ensemble where the system cell axes are fixed at the average values obtained from the NPT simulations. The simulations are then continued in an NVT ensemble for an additional 10 ps of equilibrated trajectory. Simulations containing phenol molecules are performed by first removing four H_2O molecules from our simulation cell, and second replacing them by a single C_6H_5OH molecule prior to re-equilibration of the system. This approach allows us to keep the density of the bulk liquid phase approximately constant, obviating the need to correct for pressure differentials between products and reactants. Verification that our water phase does represent a liquid phase, with the desired density of liquid water at T = 500 K and P = 4 MPa, is given in the Supporting Information (SI).

At the outset, we recognized that sampling of reactivity using explicit water molecules to represent a bulk liquid water necessitates a free energy-based approach[37] to obtain reliable, quantitative free energies of the chemical reactions. However, the relevant fluctuations of the liquid, most notably long time dielectric relaxation, is beyond the current capabilities of existing AIMD methodologies. We have, thus, chosen to provide energetics for only a small subset of reactions, particularly the first hydrogenation step and look instead at a computed potential energy surface that accounts for only the local, short time relaxation of the solvent cage around the surface bound phenol. This is achieved by calculation of reaction paths using the climbing image nudged-elastic-band method (CI-NEB)[38,39] including 7 replicas. The approach is the same as ubiquitously done for catalytic reactions at the solid/vapor interface but here we extend this approach to also include relaxation of the solvent structure along the reaction path. To do this, minimization of our CI-NEB was performed by AIMD, where each replica of the NEB is given an initial temperature of 500 K and annealed to 0 K over a time scale of 1−2 ps, leading to a residual maximum component of the forces on the atoms of less than 1 × 10^{-3} atomic units. During this relaxation, all solvent molecules are allowed to adjust their positions to accommodate the motion of the surface-bound hydrogen toward the chemisorbed phenol. This approach allows us then to account for only short time, solvent-cage relaxation about the reaction path. The time scale of annealing of the NEB has been chosen such that it is long enough to allow for the hydrogen bonds between water molecules in the liquid phase to break/reform on the order of 4−8 times (see SI for further discussion). As an additional test of this assumption we computed the NEB for the *ortho* hydrogen addition step on Pt with two different simulations where the solvent molecules in the NEB were allowed to relax over 1 and 2 ps, respectively. This resulted in a difference in reaction energy barrier of only 3 kJ/mol, indicating that our reported results are sufficiently converged with respect to the local solvent cage relaxation. We stress that the approach allows us to at least qualitatively compare reactivity in the liquid phase on the same level as is typically performed at the metal/vapor interface and to determine the main role of the solvent on the energy of these reactions.

3. RESULTS AND DISCUSSION

3.1. Microscopic Pictures of Aqueous Interfaces of Pt(111) and Ni(111). For the purposes of the following discussion we conceptually subdivide the influence of liquid water into two main effects: (a) water surrounds the involved molecules and transition states, affecting their stability (adsorption and reaction energy) on the surface, and (b) water affecting the electronic state of the metal surface, by inducing a charge migration between the metal surface and the interfacial water molecules. In order to disentangle these influences, we first investigated the interaction of water with the metal surface with four different model systems for which 1, 9, 24, and 52 water molecules are placed on the metal surface, to represent dilute vapor, a water monolayer, a water double layer, and a bulk liquid water environment, respectively. The densities of the bulk liquid water environments were about 0.9 g/cm^3 on the Pt(111) surface and 1.0 g/cm^3 on the Ni(111) surface (see SI). The single water adsorption configuration is set up such that the H−O−H plane is parallel to surface and the oxygen atom lies on top of one metal surface atom.[40−42] The liquid bulk configurations are taken by quenching a thermalized configuration from AIMD trajectories at T = 500 K to T = 0 K and the 9 and 24 molecule water layers being taken from truncations of this configuration to mono and bilayers. For these configurations we examine the impact of water adsorption on the electronic structure of the metal slab. Note, verification that the interfacial electrostatics obtained from a quenched liquid configuration as presented here is representative of that of the actual liquid at T = 500 K is presented in the SI, which also presents a detailed discussion of how the interfacial electrostatics were computed.

The adsorption energies, E_{ad}, of water on the Pt(111) and the Ni(111) surfaces are calculated in two ways using the following equations:

$$E_{ad} = [E_{n\cdot water+surface} - (E_{surface} + n\cdot E_{water})]/n \quad (1a)$$

$$E'_{ad} = [E_{n\cdot water+surface} - (E_{surface} + E_{n\cdot water})]/n' \quad (1b)$$

where $E_{n\cdot water+surface}$ is the total energy of adsorbed water molecules (n) on the Pt(111) or the Ni(111) surface; $E_{surface}$ is the total energy of the optimized Pt(111) or Ni(111) surface; E_{water} is the energy of an isolated water molecule in vacuum; $E_{n\cdot water}$ is the energy of a relaxed slab with n water molecules and n' is the number of waters that are in direct contact with the metal surface. Equation 1a represents the binding energy with respect to the vapor phase water and thus contains energetics of water−water and water−metal contacts, whereas Equation 1b reflects solely metal−water contacts. The difference between E_{ad} and E'_{ad} thus provides a measure of the water−water interaction energy. The computed vales of E_{ad} and E'_{ad} are presented in Table 1; note that the negative adsorption energy indicates favorable (exothermic) adsorption.

Table 1. Calculated Adsorption Energies (kJ/mol) of Water Molecule(s) with/without Interactions among Water Molecules (i.e. E_{ad}/E'_{ad}) on the Pt(111) and the Ni(111) Surfaces

	single 1 H_2O	monolayer (9 H_2O)	double layer (24 H_2O)	liquid (52 H_2O)
Pt(111)	−39/−39	−52/−24	−53/−22	−56/−19
Ni(111)	−19/−19	−50/−10	−50/−10	−52/−10

dx.doi.org/10.1021/ja501592y | J. Am. Chem. Soc. 2014, 136, 10287−10298

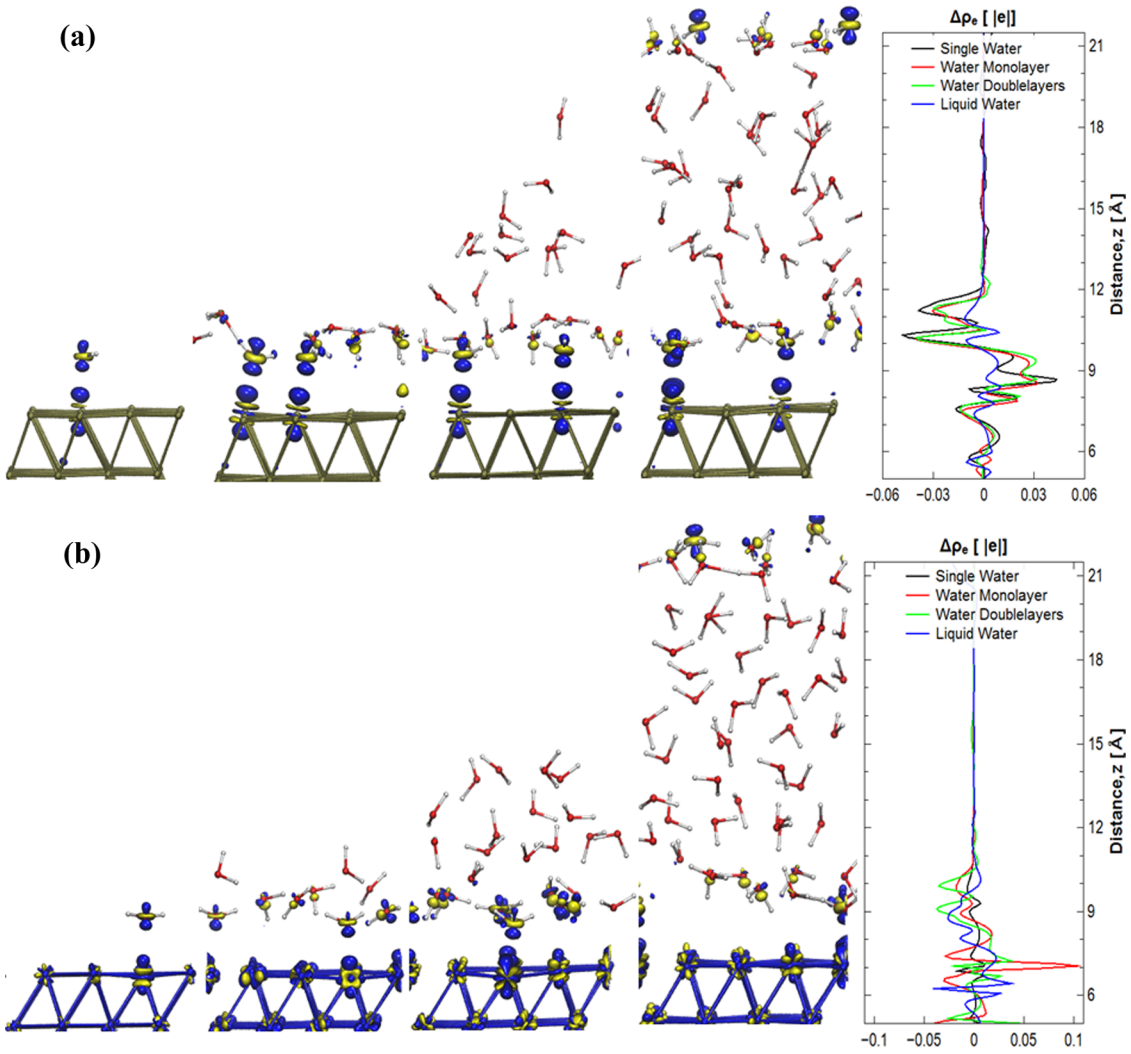

Figure 1. Electronic density difference plots for the adsorption of water molecule(s) on the Pt(111) surface (a) and the Ni(111) surface (b) with increasing number of water molecules on the surface. The far right figure is shown in one dimension along the surface normal direction. The isosurfaces are given in units of ±0.3 |e|/Bohr^3. The yellow and blue respectively represents positive and negative change difference of the electron density.

For the single water adsorption, our calculated adsorption energies are −39 and −19 kJ/mol on the Pt(111) and the Ni(111) surfaces, respectively. This interaction is best characterized as physisorption, and its magnitude is in good agreement with previous DFT calculations in which the adsorption energies are in the range of −32 ∼ −46 kJ/mol on the Pt(111) surface[40−42] and −23 ∼ −28 kJ/mol on the Ni(111) surface.[42,43] We note that the reported E_{ad} compares very well with the measured value of 47 kJ/mol reported from surface calorimetry on Pt(111).[44] But our monomer deviates from the low coverage value of 51 kJ/mol, which is most likely due to the presence of water clustering at low coverage not accounted for by the current simulations. As the water concentration on the metal surface increases, E'_{ad} essentially levels off to the averaged adsorption energy of 19 and 10 kJ/mol for Pt(111) and Ni(111) respectively, i.e., retaining the stronger binding of water to Pt relative to Ni. Likewise, the difference between E_{ad} and E'_{ad}, which measures the water−water interaction energy approaches a value of 37 and 42 kJ/mol, consistent with the enthalpy of vaporization of water between T = 0−500 K of 47−33 kJ/mol reported for the liquid phase.[45] A brief discussion of the adsorption free energy is given in the SI.

The electronic nature of aqueous H_2O/metal interfaces can be quantitatively elucidated by the change in work function W in the absence/presence of water molecules. The work function (defined as the difference of the Fermi energy and the Hartree potential (V_H) in the vacuum region; see references 46 and 47 and SI for further discussion) is directly related to chemical reactivity. It is the electronic part of the chemical potential of the metal slab and, thus, serves to measure the oxidation/reduction strength of the surface. Likewise, V_H can be used as a measure of the interfacial electrostatics and the charge motion induced by adsorption (either water and/or phenol) on the bulk metal surface.[24,46,47] The charge transfer potential, ΔV_H, is calculated by considering the difference between V_H of the total system and the sum of the potentials obtained from the isolated neutral surface slab and adsorbates (at fixed geometry). In this context, we examined the surface charge distributions at the water/metal interfaces by calculating the difference of the electron density in the presence and absence of water molecules on the surfaces by Equation 2. The charge displacement $\Delta\rho$

dx.doi.org/10.1021/ja501592y | J. Am. Chem. Soc. 2014, 136, 10287−10298

and the change in the ΔV_H are directly related by Poisson's equation:

$$\Delta\rho(x, y, z) = \Delta\rho_{n\text{-water+surface}}(x, y, z) - \Delta\rho_{\text{surface}}(x, y, z) - \Delta\rho_{n\text{-water}}(x, y, z) \quad (2)$$

$$\Delta\rho(x, y, z) = -\frac{\nabla V_H(x, y, z)}{4\pi\varepsilon_0} \quad (3)$$

where $\Delta\rho(x,y,z)$ is the electron density difference in Cartesian space. This approach provides a quantitative mapping between adsorption induced charge motion and the change of W due to adsorption, and, hence, the change of oxidation/reduction strength. Decomposition in terms of ΔV_H and $\Delta\rho$ allows us to unambiguously identify charge transfer by directly accessing the electrostatic terms within the Hamiltonian, circumventing the prejudices of various population analysis methods. In particular, we project the electron density difference along the surface normal direction (z) by integration $\Delta\rho(z) = \int\int dxdy{\cdot}\Delta\rho(x,y,z)$. The resulting $\Delta\rho(x,y,z)$ (as an isosurface) and $\Delta\rho(z)$ for both the H_2O/Pt(111) and the H_2O/Ni(111) interfaces are shown in Figure 1a,b. In general, we note that the result of water adsorption is the displacement, back toward the surface, of the diffuse electron density tail of the metal via Pauli repulsion by the electrons of the physisorbed water, which is a well-known effect in surface physics.[46,48] This response is principally due to the fact that the strength of the induced polarization depends on the number of water molecules involved. The change in W upon adsorption will also depend on whether or not a preferred orientation of the molecular dipole moment exists.[40,49] We note, however, that we do not see evidence for preferred orientation of water molecules at the interface in the current AIMD simulations at T = 500 K. The net result is that metal electron density is pushed into the surface and piles up at the subsurface layer leading to an induced surface dipole, with negative end oriented toward the surface, growing as the water coverage increases.

As noted above, our calculated W for the clean Pt and Ni surfaces (5.6 and 4.9 eV) are slightly underestimated compared to the experimental values due to the small unit cells needed for efficient AIMD simulations with a liquid water phase.[50,51] With the single adsorbed water on the surfaces, the work functions of Pt and Ni surfaces decreased slightly to 5.3 and 4.8 eV respectively. This effect increases steadily as one goes from the monolayer up to the bulk liquid, such that W is reduced by 1.2 and 1.0 eV for Pt and Ni, respectively. We note that our disordered monolayer result shows a decrease of W on Pt(111) of 0.6 eV in good agreement with the 0.7−0.8 eV experimentally measured for well-ordered 1 ML coverage water films.[52] Indeed the magnitude of reduction of W resulting from Pauli repulsion estimated here is similar to that reported for other systems such as Xe/Cu or dimethydithiol/Au(111) at full adsorbate coverage, indicating that this effect is relatively independent of the identity of adsorbate and metal surface.[46,48]

We note that the computed ensemble average electron density shift, $\Delta\rho(z)$ (and hence shift in W) obtained from sampling trajectories at T = 500 K are essentially identical for the representative quenched structures presented above (see Figure S3 and the related discussion in SI). Thus, it can be concluded that the computed reductions in W for both Pt(111) and Ni(111) will be present at elevated temperatures in the presence of the liquid phase.

The significance of the above findings is that the redox chemistry of the Pt and the Ni are markedly changed by the influence of the solvent such that the energy cost to reduce/oxidize an adsorbate (remove/add electron density from the metal) is markedly different from that at the metal/vapor interface by approximately 1 eV.[53] The impact of this observation on adsorbate binding and stabilization of reaction intermediates is the focus of the next subsections.

3.2. Effects of Aqueous Environments on the Phenol Adsorption. We find, in agreement with previous DFT calculations,[20,22] that in the absence of water the most stable adsorption configurations of phenol on the Pt(111) and the Ni(111) surfaces are very similar, i.e., the parallel geometries at the 3-fold hollow sites shown in Figure 2a,c. The calculated adsorption energies of phenol are −172 and −96 kJ/mol on the Pt(111) and Ni(111) surfaces, respectively. Although our calculated adsorption energy of phenol on the Ni(111) surface

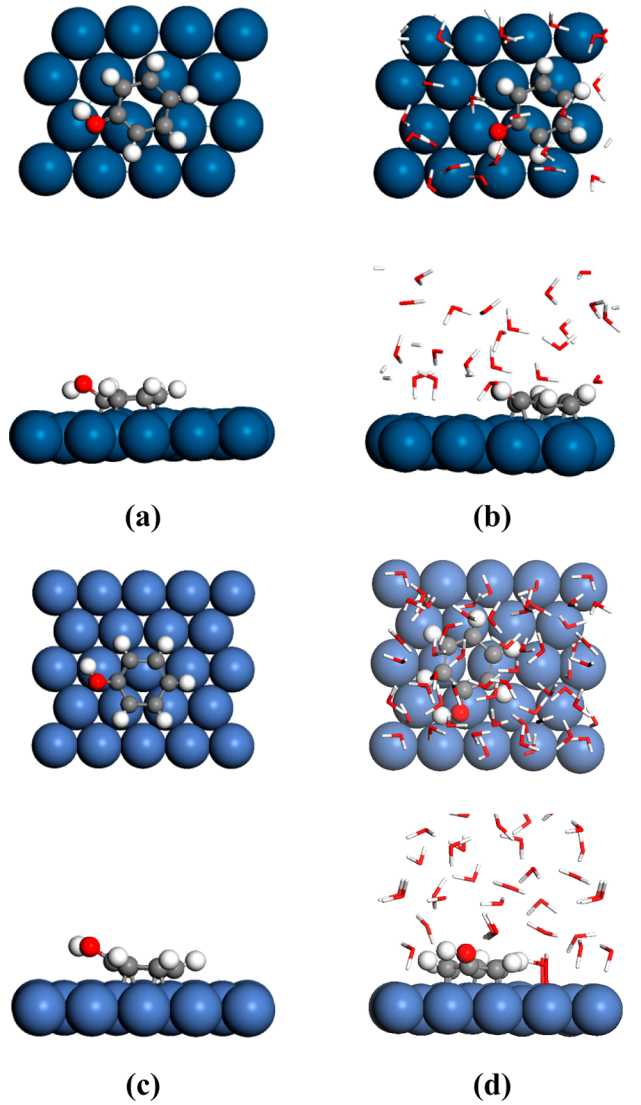

Figure 2. Optimized structures of the adsorbed phenol on the metal surfaces in vacuum and water environments. (a) in vacuum over Pt(111); (b) in liquid water over Pt(111); (c) in vacuum over Ni(111); (d) in liquid water over Ni(111). The Pt and Ni atoms are in dark and light blue; the O, H, and C atoms are in red, white, and gray, respectively.

dx.doi.org/10.1021/ja501592y | J. Am. Chem. Soc. 2014, 136, 10287−10298

agrees well with the previous result of −86 kJ/mol,[20] the calculated adsorption energy of phenol on the Pt(111) surface is appreciably lower than the reported DFT value of −215 kJ/mol which was obtained at a lower surface coverage.[22] As seen in Figure 2a, the OH group of the adsorbed phenol is tilted away from the Pt(111) surface. As a result, the hydroxyl-bonded C atom on the phenolic ring is much farther away from the surface than other C atoms on the phenolic ring. The distances between the C atom connected to the OH group and the two closest surface Pt atoms are 2.67 and 2.70 Å, which is longer than the previously reported bonded length of 2.28 Å.[22] For the other five C atoms, the calculated bond lengths are 2.16−2.22 Å, which are in good agreement with previous values.[22] With adsorbed phenol on the Ni(111) surface the OH group of phenol is even farther away from the surface as shown in Figure 2c. The distances between the C atom connected with the OH group and the two closest surface Ni atoms are 2.81 and 3.07 Å, while the distances between the other five C atoms and the closest surface Ni atoms are 2.14−2.20 Å, consistent with previous DFT results.[20] The obtained shorter distances between C on the phenolic ring and the adjacent Pt atoms indicate stronger interactions between phenol and Pt than between phenol and Ni.

To investigate the effect of an aqueous environment on the adsorption of phenol on Pt(111) and Ni(111) surfaces, a model system with 48 water molecules and one adsorbed phenol on the (111) surface was chosen. The entire model system was initially equilibrated for 5 ps at 500 K using AIMD simulations. An equilibrated configuration was then extracted by quenching the equilibrated H_2O/phenol/metal system trajectories. For the aqueous phase we compared the energetics between the adsorbed phenol on the surface and a configuration separately prepared in a similar manner, where phenol was constrained to be within the center of the water bulk slab allowing the water molecules to relax and form a solvent cage around the phenol. The optimized geometry of adsorbed phenol on the Pt(111) and the Ni(111) surfaces are shown in Figure 2b,d. The adsorption energies of phenol in liquid water were found to be −151 and −85 kJ/mol on the Pt(111) and Ni(111) surfaces, respectively. The net decrease in phenol adsorption energy induced by the presence of water is thus only 10−20 kJ/mol.

Examining the change in W accompanying adsorption of phenol allows one to follow surface charge rearrangement. For the Pt(111) and the Ni(111) surfaces in the absence of water, phenol adsorption leads to a decrease in W by 0.2 and 0.7 eV, respectively, relative to the values calculated for these surfaces in the aqueous phase. A decrease in W implies an induced surface dipole layer, in which the net electron density moves away from phenol toward the metal, i.e., effectively an oxidation of phenol at the metal surface.[46,48] A comparable electronic chemical potential for phenol can be estimated for phenol (in the gas phase) by a Mullikan electronegativity approximation,[54] $-(I + A)/2$, where I is the ionization energy and A the electron affinity. For phenol we calculate that W is 3.3 eV, which is comparable to the value of 3.8 eV estimated from experimental measurements.[55] Since that value is appreciable lower than W for either metal surface, it could have been assumed that net charge is transferred from phenol to Ni and, to a greater extent, to Pt upon adsorption. Figure 3 shows that charge density as represented by $\Delta\rho(z)$ is transferred from the molecule into the surface regardless of whether the surface contacts a liquid or gaseous environment.

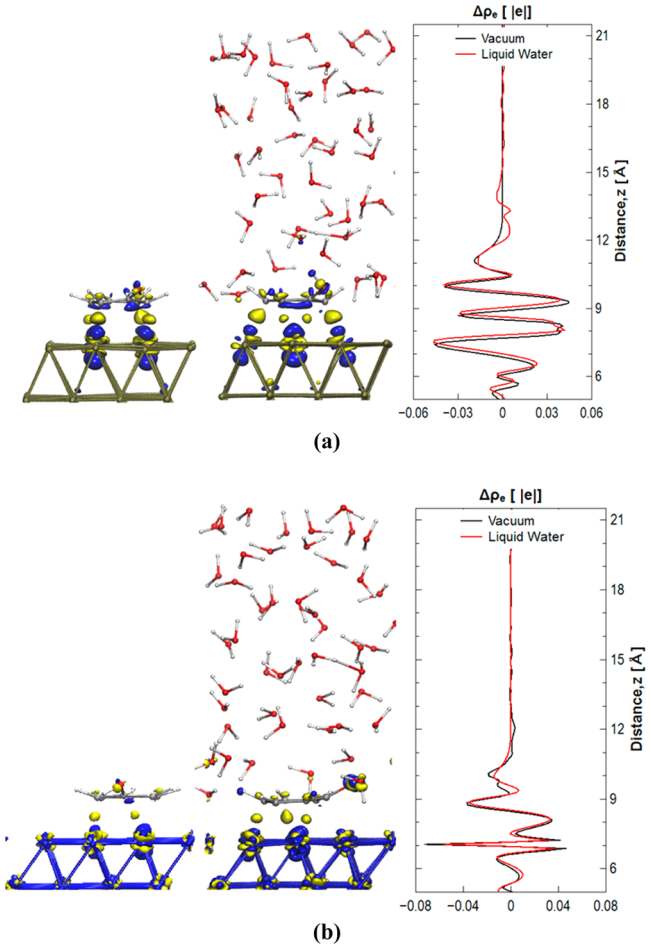

Figure 3. Electron density difference plots for the adsorption of phenol on the Pt(111) surface (a) and the Ni(111) surface (b) with increasing number of water molecules on the surface. The color scheme is that of Figure 1.

We summarize our results in a thermodynamic cycle in Scheme 2. Note that the solvation enthalpy of phenol in water

Scheme 2. Thermodynamic Cycle for Phenol Adsorption (C_6H_5OH*) on Pt(111) or Ni(111) in Vapor and Liquid Phases

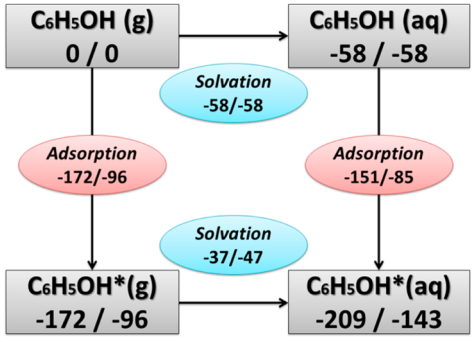

is 58 kJ/mol[56] relative to a phenol in the gas phase. Thus, with respect to a gas phase reference, the adsorption enthalpy of phenol on the hydrated metal surface is larger than at the solid/vapor interface by −37 and −47 kJ/mol for Ni and Pt, respectively. We note that, qualitatively, one would expect that solvation of a partially positively charged adsorbed phenol

dx.doi.org/10.1021/ja501592y | J. Am. Chem. Soc. 2014, 136, 10287−10298

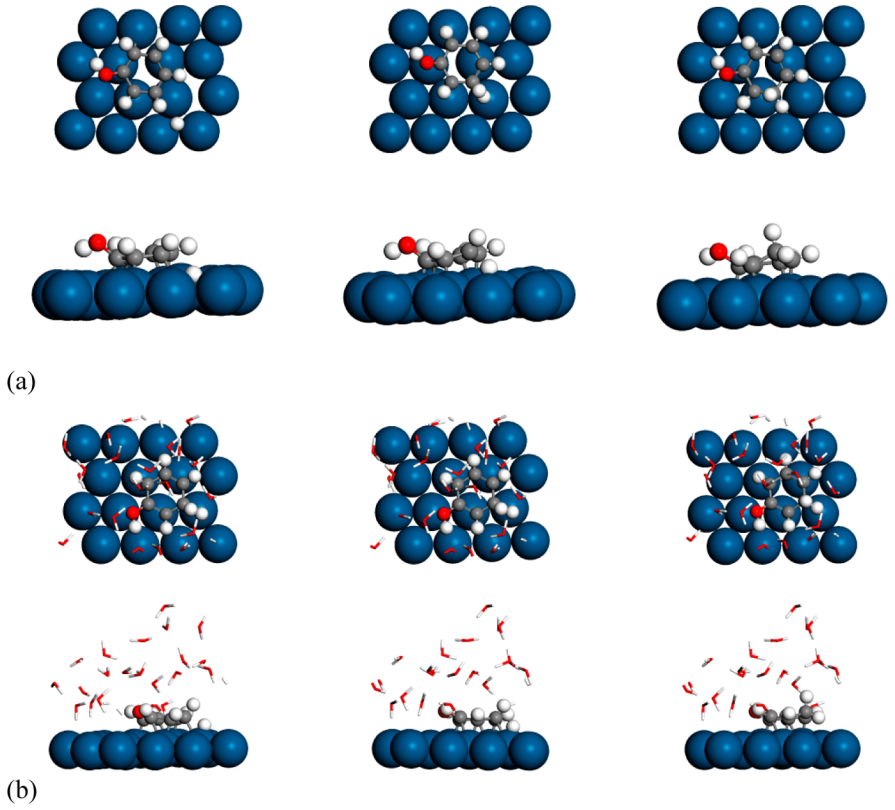

Figure 4. Optimized structures of phenol first hydrogenation to cyclohexadienyl radical at the *meta* C positions on the Pt(111) surface in vacuum (a) and in liquid water (b).

should be stronger than of a neutral species; however, the surface-bound species are only partially solvated. The result is a balance between two opposing effects that decreases the solvation energy for the adsorbed species on both Pt(111) and Ni(111) by 21 and 11 kJ/mol, respectively. Overall, it is clear that the binding of this prototypic, polar organic to metal surfaces can be influenced by both changes in electronic nature of the metal upon solvation and the solvation energy of the adsorbed species. As shown below this has a strong influence on the relative energetics of reaction intermediates for the phenol hydrogenation process.

3.3. Phenol Hydrogenation in the Presence of Liquid Water. As suggested by previous DFT studies,[27,28] the existence of an aqueous solvent phase can also affect the surface reaction by changing the stabilities of reactants, products, and transition state. As a result, the surface reaction might shift from energetically favorable (exothermic) to unfavorable (endothermic), determined by the relative stabilities of the initial state (reactants) and the final state (products). Most importantly, the activation barriers of the surface reactions vary with the relative stabilities between the initial and the transition states. The effect of the aqueous phase on the phenol hydrogenation was examined by studying the addition of the first and second H adatoms to phenol adsorbed on Pt(111) and Ni(111) surfaces in the vapor and liquid water phase (explicitly represented by 48 water molecules). The addition of two H atoms to phenol produces isomers with distinguishable C positions of the phenolic ring being saturated.

We consider the nature of the charge state and location of the surface H adatom in the hydrogenation process at low H coverage condition. A detailed study of the H coverage and various locations on the phenol hydrogenation is beyond the scope of the current work. In comparing the vapor/metal and liquid/metal interface, we examine the energetics (denoted ΔE_H) for an H adatom located on the surface versus in the first subsurface layer. For Ni(111) and Pt(111) surfaces, a single H adatom is found to prefer a surface site with $\Delta E_H = -87$ and -67 kJ/mol, respectively. The same energy preference is retained in the liquid phase, although the energy difference ΔE_H is lowered by ~10 kJ/mol. The adsorption of phenol is found to have negligible impact on this process. The change in the interfacial electronic structure associated with adding H to the surface is only a small shift of electronic density away from H toward the metal leaving a negligibly small positive charge on H. This in effect has almost no impact on the work function, which is lowered by at most 0.1 eV. Thus, the adsorbed H residing on both Pt and Ni surfaces can be considered to be effectively a neutral H adatom.

As the major objective of this study is to understand the impact of the aqueous phase on the hydrogenation of phenol on Pt and Ni, we place a single H adatom on the surface adjacent to *ortho*, *meta*, or *para* CH group of the phenolic ring (see Scheme 1b). Three hydrogenation paths leading to an adsorbed cyclohexadienyl radical intermediate were calculated with a resulting CH_2 group at *ortho*, *meta*, and *para* positions. We performed searches for the direct addition of H to phenol as well as solvent-mediated proton-transfer pathways; however the latter were found to be appreciably higher in activation energy (ca. ~90 kJ/mol) and will be omitted from the subsequent discussions. We note that, variation of the energetics associated with the adsorbed H relative to the different C positions is on the order of 10 kJ/mol, indicating that there is little effect from steric hindrance or anisotropy in the charge distribution. Figure 4 graphically displays the

dx.doi.org/10.1021/ja501592y | J. Am. Chem. Soc. 2014, 136, 10287−10298

products, reactants and transition states for the hydrogen adatom addition step to the *meta* C position on the Pt(111) surface for both the gas and liquid phase.

Comparative energy landscapes for hydrogen adatom addition are given in Figure 5 for the vapor phase and Figure 6 for the liquid phase. At the vacuum/metal interface, first phenol hydrogen adatom addition at the *ortho* position is found to have the lowest activation energy ΔE^{*}_{HYD} for both Pt(111) and Ni(111) surfaces among three possible positions. The calculated values of ΔE^{*}_{HYD} at the *ortho* position are nearly the same on the Pt(111) (94 kJ/mol) and the Ni(111) surface (96 kJ/mol). As shown in Figure 6, all three cyclohexadienyl radical products are endothermic for Ni and Pt surfaces. Analysis of each transition state suggests that very little charge builds up on H, which indicates that the H adatom addition at the vapor/metal interface is H atom transfer. As measured by the Bader charge analysis method,[57,58] the H adatom has a partial charge of approximately +0.12 |e|, which does not change in the transition state for both metal surfaces regardless of the absence or the presence of water. However, the final cyclohexadienyl radical intermediate shows an enhanced positive charge suggesting that hydrogenation is followed by further donation of electron density to the surface.

The presence of liquid water has little effect on the selectivity of the first hydrogen adatom addition to phenol on both Ni and Pt surfaces. In both cases, addition at the *ortho* position is preferred. It is found that the activation barrier for the *ortho* position H adatom addition only decreases by 13 kJ/mol on Pt(111) and by 4 kJ/mol on Ni(111). Although all three pathways are still endothermic on both metal surfaces, the liquid phase has pronounced effect on the hydrogenation barriers for the other two C (*meta* and *para*) position on the Ni(111) stabilizing them by about 20 kJ/mol. On the other hand, the activation energies on Pt(111) (see Figure 6) are essentially the same in presence and absence of liquid water. As noted above, charge analysis of the H adatom at the transition state suggests that the adsorbed H adatom is only partially positively charged such that the H addition in liquid water remains a H atom transfer, whose transition state is only weakly stabilized by the surrounding water molecules. In general, the solvation of the H adatom perturbs the hydrogenation only slightly, because the hydrophobic H adatom[59] has only weak interactions with water at the interface between the surface and adsorbed phenol. We note that water-mediated, H adatom addition (which is actually a proton transfer followed by electron transfer from the metal) to the adsorbed phenol did not occur in any of our simulations. Overall for this reaction step, there are only minor changes in the activation energies relative to the vapor phase. On the other hand, the relative energetics of the final products of first H adatom addition step are influenced by water solvation by 10 kJ/mol on the Pt(111) surface, and the products for the *meta* and the *para* positions on the Ni(111) surface are stabilized appreciably. For the Ni(111) surface the reaction energies for the first H adatom addition step on the *meta* and the *para* positions decrease from +117 and +121 kJ/mol in gas phase to +67 and +41 kJ/mol in the presence of liquid water. As noted above, these products have

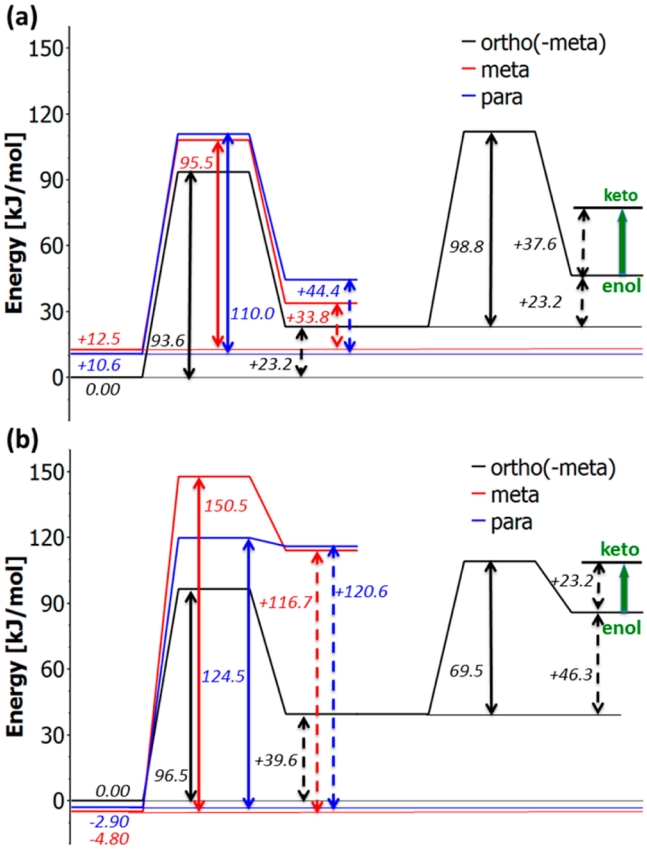

Figure 5. Reaction energy profiles of the first and the second hydrogen atom addition steps of phenol on (a) Pt(111) and (b) Ni(111) in the vapor phase. Compare with Figure 6 for concurrent metal/aqueous interface results.

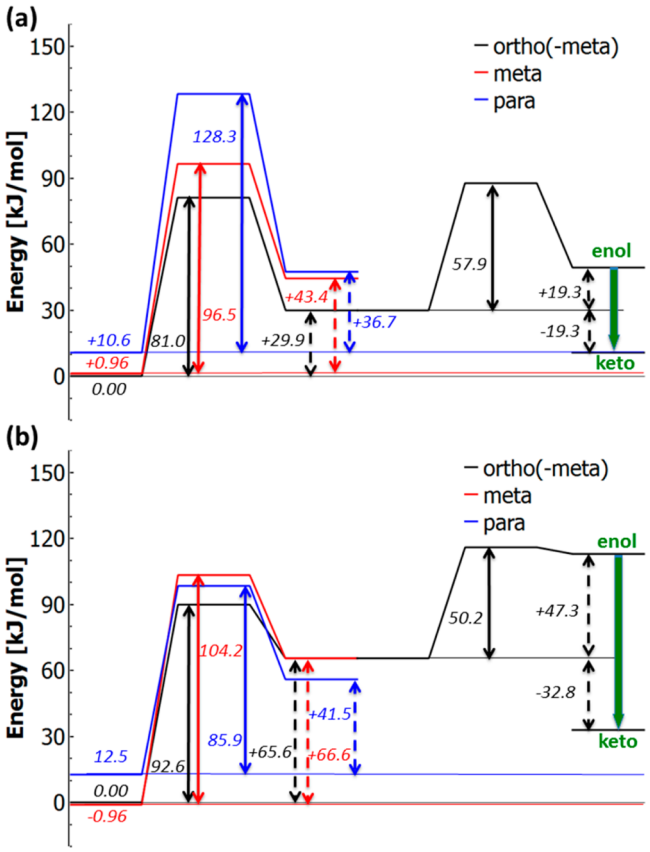

Figure 6. Reaction energy profiles of the first and the second hydrogen addition steps of phenol on (a) Pt(111) and (b) Ni(111) in the liquid water phase. Compare with Figure 5 for concurrent reactions at the metal/vapor interface.

dx.doi.org/10.1021/ja501592y | J. Am. Chem. Soc. 2014, 136, 10287−10298

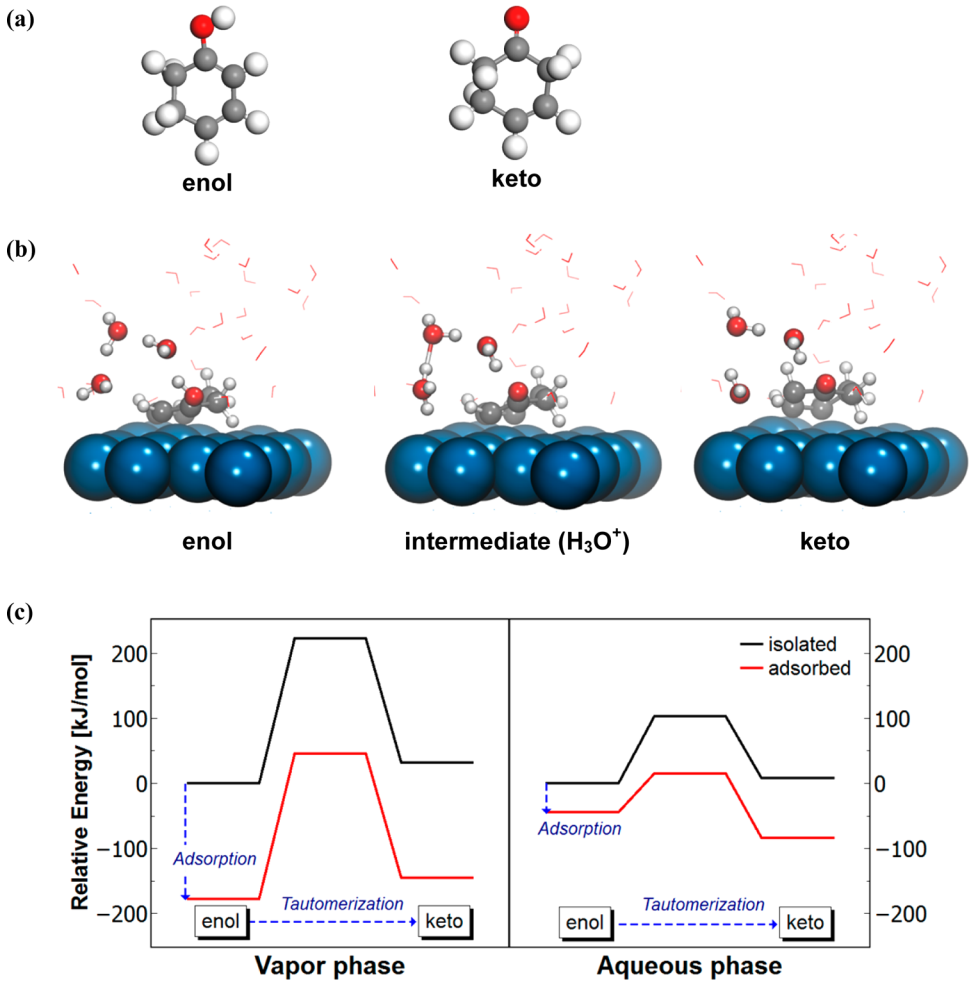

Figure 7. (a) Optimized structures of 1,3-cyclohexadienol (enol) and 3-cyclohexenone (keto) isomers in the gas phase. (b) Water-assisted proton exchange reaction path on Pt(111) in aqueous phase starting from structures of enol (left), intermediate with solvated H_3O^+ (center), and keto form (right). Only waters directly linked to proton transfer pathway are shown. (c) Schematic of relative energies for enol/keto tautomerization at metal/vapor (left) and metal/aqueous (right) interfaces.

partial positive charges, due to enhanced adsorbate-to-metal charge transfer relative to phenol, leading to the enhanced stabilization of the intermediates.

Our first hydrogen adatom addition results show the *ortho* C position of the phenolic ring is slightly preferred over the *meta* and the *para* positions on both Pt and Ni. Therefore, the second hydrogen addition step is investigated by adding another H adatom to the neighboring *meta* C position of *ortho* cyclohexadienyl radical intermediate to create an adsorbed 1,3-cyclohexadienol intermediate (see Figure S5 in SI for graphical representation). The calculated activation energy barriers are 99 and 70 kJ/mol leading to products which are endothermic by 46 and 23 kJ/mol respectively for Pt(111) and Ni(111) respectively. We note that the second hydrogen adatom addition step on both surfaces is very similar to the first in the vapor phase in that both are energetically uphill processes. The only appreciable difference is that the activation barrier on the Ni(111) surface becomes lower. However, in the presence of liquid water, our results show that both activation barriers for the second hydrogen adatom addition decrease pronouncedly to 58 and 50 kJ/mol, while the reaction energies of the second hydrogenation step are still endothermic with +46 and +19 kJ/mol on the Pt(111) and Ni(111) surfaces, respectively. Here too, the liquid water environment plays a role in the stabilization of surface-bound intermediates, but does not alter the overall energetic uphill nature of the reaction path.

On the other hand, we find that the produced 1,3-cyclohexadienol from the second hydrogen adatom addition only weakly binds to the Pt and Ni surface. Compared to the strong binding of 1,3-cyclohexadienol in the presence of gas phase (−178 kJ/mol for Pt(111) and −86 kJ/mol for Ni(111)), the computed adsorption energies of 1,3-cyclohexadienol (relative to a solvated species) are only −48 and −12 kJ/mol on the Pt and Ni surfaces in liquid water. This weak interaction between the formed enol species and metal surface suggests that, at T = 500 K, the enol species might desorb from the surface into the liquid water before further hydrogenation. In other words, one might expect that the 1,3-cyclohexadienol could be one of the major products like cyclohexanone during aqueous phase phenol hydrogenation. However, in place of the desorption from the surface, the produced 1,3-cyclohexadienol rapidly undergoes keto/enol tautomerization.[60] In the fully solvated aqueous environment we calculate that the enol form is more stable than the keto form by 8 kJ/mol suggesting the desorbed molecule would at best establish a keto/enol equilibrium. In this context, Dzingeleski et al. found that 1,3-cyclohexadienol is readily ketonized to the unconjugated ketone 3-cyclohexenone (major product) and the conjugated

dx.doi.org/10.1021/ja501592y | J. Am. Chem. Soc. 2014, 136, 10287−10298

ketone 2-cyclohexenone (minor product).[60] In the present work, we find the unconjugated 3-cyclohexenone (keto) adsorbed on Pt and Ni surfaces (Figure 7), derived from the tautormerization of the adsorbed 1,3-cyclohexadienol, is energetically more stable than its enol form (1,3-cyclohexadienol) but only in the presence of liquid water; see Table 2. At the solid/liquid interface the keto isomer is stabilized relative to the enol form by 38 and 80 kJ/mol on the Pt(111) and the Ni(111) surfaces respectively with the calculated adsorption energies of 3-cyclohexenone (keto) on the Pt(111) and Ni(111) surface are −92 and −143 kJ/mol, respectively. Whereas at the vapor/solid interface the keto is bound by 140 and 63 kJ/mol to Pt(111) and Ni(111) respectively and is, therefore, destabilized with respect to the adsorbed enol form. Hence, the enthalpic driving force for the keto/enol isomerization is the highest when the molecule is adsorbed at the metal surface in the aqueous phase.

Table 2. Calculated Reaction ($\Delta E_{reaction}$) and Activation ($\Delta E^{*}_{activation}$) Energies (kJ/mol) for Isomerization of 1,3-Cyclohexadienol to 3-Cyclohexenone on the Pt(111)/Ni(111) Surfaces in Both the Vapor and Aqueous Phase

	Pt(111)		Ni(111)			
	(vapor)	(aqueous)	(vapor)	(aqueous)	gas phase	aqueous phase
$\Delta E_{reaction}$	38	−39	23	−80	32	8
$\Delta E^{*}_{activation}$	184	121/59[a]	106	71/63[a]	223	102

[a]Proton transfer via surface/water.

We now discuss in detail the computed energy barriers for the enol/keto isomerization, (Table 2 and Figure 7). The activation energy for the enol to keto isomerization by a direct proton transfer from the oxygen to the carbon is 223 kJ/mol for gas phase 1,3-cyclohexadienol. This reaction in the liquid phase has an appreciably reduced barrier of 102 kJ/mol due to the stabilization of the proton by the solvating water molecules one of which forms a hydronium ion at the transition state. This is in line with the reaction being relatively fast in the aqueous phase with the isomers in thermal equilibrium.[61] Enol/keto isomerization at the gas/solid interface has a reduced energy barrier of 184 and 106 kJ/mol for Pt(111) and Ni(111) respectively. This barrier is reduced relative to that of the isolated gas phase molecule as a result of the proton, at the transition state, being partially stabilized by a direct interaction with the metal. The same reaction path in the presence of water is further lowered with barriers of 121 and 71 kJ/mol on Pt(111) and Ni(111) respectively due to a further stabilization of the transition state by the solvating water molecules. However, this reaction channel is no longer the lowest energy path for establishing the enol/keto isomerization. Unlike, the H-adatom addition steps, the aqueous solvent can directly participate in the reaction by establishing a Grotthuss proton transfer chain, in which the alcohol group of 1−3-cyclohexadienol is deprotonated by a nearby water molecule forming a solvated hydronium ion intermediate (see Figure 7b). In a second step, a series of synchronous proton transfers, among up to 3 water molecules, results in a proton from water being transferred back to the adsorbed organic to form 3-cyclohexenone. This Grotthuss mechanism has an overall reaction energy barrier of 59 and 63 kJ/mol for Pt(111) and Ni(111) respectively. Moreover, the expectation is that this later mechanism would be enhanced in rate as the pH of the water is reduced due to an increased population of H_3O^+ species which could further catalyze this transformation.[60] As such there is a greater probability that the 3-cyclohexenone can either remain adsorbed or potentially readsorb to the metal for further hydrogenated toward cyclohexanone and cyclohexanol.

Returning to our original question regarding potential mechanistic routes raised in Section 1, we conclude that hydrogenation at the metal/aqueous interface must proceed via a cyclohex-3-enone intermediate, due to rapid keto/enol isomerization, and can undergo further hydrogenated to cyclohexanone (see upper route in Scheme 3). At the solid/vapor interface the keto/enol equilibrium is thermodynamically unfavorable and kinetically hindered. As such, that phenol will remain on the surface for further hydrogenation to cyclohexanol (lower route in Scheme 3). This mechanistic route for vapor phase hydrogenation is in agreement with past work on hydrogenation on a sulfided CoMo catalyst[14] in this same environment (when one factors in that acid catalyzed steps on metal surfaces are unlikely). Overall, we find that at both the solid/vapor and solid/aqueous interface the H adatom addition is a neutral H atom transfer (not a proton H^+ or a hydride H^- transfer). As such, there is only a weak influence of water on the reaction energy barriers for the hydrogenation. On the other hand, proton transfer reactions are strongly influenced by the aqueous environment and hence reactions such as keto/enol isomerization (even for adsorbed species) experience appreciably lower activation energies. More importantly, the major influence of the liquid is upon the relative energetics of charged surface bound intermediates. In the particular case of phenol hydrogenation this results in a shift toward the energetic preference to form ketones.

Scheme 3. Proposed Phenol Hydrogenation Pathways Resulting from the Current Study in Aqueous Liquid Phase (upper route) and Vapor Phase (lower route)

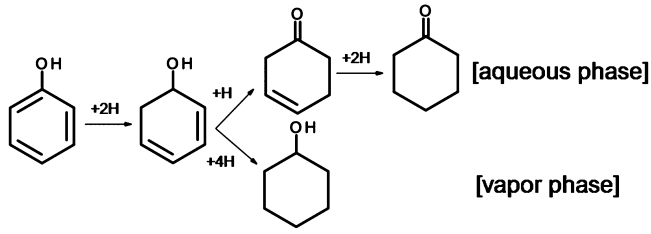

4. CONCLUSIONS

The major change in the DFT electronic structure calculations of both Pt(111) and Ni(111), between a vapor- and liquid-phase surrounding, results from a redistribution of the diffuse tail of electron density emanating from the metal surface to lower energies, which in turn lowers the metal work function by about 1 eV. The smaller work function makes the metal a stronger chemical reducing agent and a poorer oxidizing agent. In the case of phenol adsorption from water, the decreased work function lowers the phenol adsorption energy, despite a stabilizing influence of the solvation of the partly charged adsorbate. We anticipate that binding for species that are reduced upon adsorption, however, should be enhanced. The reaction barriers for adding surface-bound H adatoms to phenol is lowered by only 10−20 kJ/mol, due to a small stabilizing influence of charge at the transition state. Platinum group metals catalyzing hydrogenation reactions, should all exhibit

this relatively small influence on hydrogenation activation barriers for aqueous phase reactions. On the other hand, keto/enol isomerization of surface bound intermediates, such as 1,3-cyclohexadienol, is strongly influenced by the solvent both in terms of stabilization of the surface bound keto form as well as an appreciable lowering of the activation energy for the proton transfer which occurs at the transition state of the tautomerization reaction.

A more quantitative correlation between this effect and the liquid phase work function of the metal surface (e.g., linear free energy relationships) is both beyond the scope of the current work and would necessitate a larger ensemble of representative reactions. Due to the difficulty associated with obtaining reliable free energetics for these processes, the current work has focused on the enthalpic/energetic impact of the solvation. The evaluation of the role of entropy at the solid/liquid interface and its impact on the global kinetics of the liquid phase hydrogenation process will be the focus of subsequent studies.

■ ASSOCIATED CONTENT

Supporting Information

Validation of liquid state of water environment, and optimized structure of reactant, product and transition state for the second hydrogenation of cyclohexadienyl to 1,3-cyclohexadienol. This material is available free of charge via the Internet at http://pubs.acs.org.

■ AUTHOR INFORMATION

Corresponding Authors

donghai.mei@pnnl.gov
roger.rousseau@pnnl.gov
Johannes.lercher@pnnl.gov

Notes

The authors declare no competing financial interest.

■ ACKNOWLEDGMENTS

This work was supported by the US Department of Energy, Y.Y., D.H.M., and J.L. were supported by Office of Basic Energy Sciences, Division of Chemical Sciences, Geosciences & Biosciences and R.R. and R.S.W. were supported by Office of Energy Efficiency and Renewable Energy, Bioenergy Technologies Office. Pacific Northwest National Laboratory (PNNL) is a multiprogram national laboratory operated for DOE by Battelle under contract AC0676RLO1830. Computing time was granted by the grand challenge of computational catalysis of the William R. Wiley Environmental Molecular Sciences Laboratory (EMSL) and by the National Energy Research Scientific Computing Center (NERSC), which is supported by the Office of Science of the U.S. Department of Energy under Contract No. DE-AC02-05CH11231. EMSL is a national scientific user facility located at Pacific Northwest National Laboratory (PNNL) and sponsored by DOE's Office of Biological and Environmental Research.

■ REFERENCES

(1) Huber, G. W.; Iborra, S.; Corma, A. *Chem. Rev.* **2006**, *106*, 4044–4098.
(2) He, J.; Zhao, C.; Lercher, J. A. *J. Am. Chem. Soc.* **2012**, *134*, 20768–20775.
(3) Peng, B.; Yuan, X.; Zhao, C.; Lercher, J. A. *J. Am. Chem. Soc.* **2012**, *134*, 9400–9405.
(4) Wang, Y.; Yao, J.; Li, H.; Su, D.; Antonietti, M. *J. Am. Chem. Soc.* **2011**, *133*, 2362–2365.
(5) Zapata, P. A.; Faria, J.; Ruiz, M. P.; Jentoft, R. E.; Resasco, D. E. *J. Am. Chem. Soc.* **2012**, *134*, 8570–8578.
(6) Zheng, Y.; Jiao, Y.; Chen, J.; Liu, J.; Liang, J.; Du, A.; Zhang, W. M.; Zhu, Z. H.; Smith, S. C.; Jaroniec, M.; Lu, G. Q.; Qiao, S. Z. *J. Am. Chem. Soc.* **2011**, *133*, 20116–20119.
(7) Crossley, S.; Faria, J.; Shen, M.; Resasco, D. E. *Science* **2010**, *327*, 68–72.
(8) Huber, G. W.; Chheda, J. N.; Barrett, C. J.; Dumesic, J. A. *Science* **2005**, *308*, 1446–1450.
(9) Liu, H.; Jiang, T.; Han, B.; Liang, S.; Zhou, Y. *Science* **2009**, *326*, 1250–1252.
(10) Elliott, D. C. *Ener. Fuels* **2007**, *21*, 1792–1815.
(11) Furimsky, E. *Appl. Catal., A* **2000**, *199*, 147–190.
(12) Zhao, C.; Kou, Y.; Lemonidou, A. A.; Li, X.; Lercher, J. A. *Angew. Chem., Int. Ed.* **2009**, *48*, 3987–3990.
(13) Hong, D.-Y.; Miller, S. J.; Agrawal, P. K.; Jones, C. W. *Chem. Commun.* **2010**, *46*, 1038–1040.
(14) Massoth, F. E.; Politzer, P.; Concha, M. C.; Murray, J. S.; Jakowski, J.; Simons, J. *J. Phys. Chem. B* **2006**, *110*, 14283–14291.
(15) Hummelshoj, J. S.; Abild-Pedersen, F.; Studt, F.; Bligaard, T.; Norskov, J. K. *Angew. Chem., Int. Ed.* **2012**, *51*, 272–274.
(16) Neurock, M. *Ind. Eng. Chem. Res.* **2010**, *49*, 10183–10199.
(17) Neurock, M.; Wasileski, S. A.; Mei, D. *Chem. Eng. Sci.* **2004**, *59*, 4703–4714.
(18) Norskov, J. K.; Scheffler, M.; Toulhoat, H. *MRS Bull.* **2006**, *31*, 669–674.
(19) Jenkins, S. J. *Proc. R. Soc. A* **2009**, *465*, 2949–2976.
(20) Delle Site, L.; Alavi, A.; Abrams, C. F. *Phys. Rev. B* **2003**, *67*, 193406.
(21) Ghiringhelli, L. M.; Caputo, R.; Delle Site, L. *Phys. Rev. B* **2007**, *75*, 113403.
(22) Honkela, M. L.; Bjork, J.; Persson, M. *Phys. Chem. Chem. Phys.* **2012**, *14*, 5849–5854.
(23) Calle-Vallejo, F.; Koper, M. T. M. *Electrochim. Acta* **2012**, *84*, 3–11.
(24) Schnur, S.; Gross, A. *New J. Phys.* **2009**, *11*, 125003.
(25) Taylor, C. D.; Neurock, M. *Curr. Opin. Solid State Mater. Sci.* **2005**, *9*, 49–65.
(26) Zope, B. N.; Hibbitts, D. D.; Neurock, M.; Davis, R. J. *Science* **2010**, *330*, 74–78.
(27) Desai, S. K.; Pallassana, V.; Neurock, M. *J. Phys. Chem. B* **2001**, *105*, 9171–9182.
(28) Desai, S. K.; Neurock, M. *Phys. Rev. B* **2003**, *68*, 075420.
(29) CP2K code and reference material is available at the project web page: http://www.cp2k.org.
(30) VandeVondele, J.; Hutter, J. *J. Chem. Phys.* **2007**, *127*, 114105.
(31) Lippert, G.; Hutter, J.; Parrinello, M. *Mol. Phys.* **1997**, *92*, 477–487.
(32) Krack, M. *Theor. Chem. Acc.* **2005**, *114*, 145–152.
(33) Goedecker, S.; Teter, M.; Hutter, J. *Phys. Rev. B* **1996**, *54*, 1703–1710.
(34) Grimme, S.; Antony, J.; Ehrlich, S.; Krieg, H. *J. Chem. Phys.* **2010**, *132*, 154104.
(35) Baker, B. G.; Johnson, B. B.; Maire, G. L. C. *Surf. Sci.* **1971**, *24*, 572.
(36) Derry, G. N.; Zhang, J. Z. *Phys. Rev. B* **1989**, *39*, 1940–1941.
(37) Limmer, D. T.; Willard, A. P.; Madden, P.; Chandler, D. *Proc. Natl. Acad. Sci. U.S.A.* **2013**, *110*, 4200–4205.
(38) Henkelman, G.; Uberuaga, B. P.; Jonsson, H. *J. Chem. Phys.* **2000**, *113*, 9901–9904.
(39) Mills, G.; Jonsson, H.; Schenter, G. K. *Surf. Sci.* **1995**, *324*, 305–337.
(40) Gohda, Y.; Schnur, S.; Gross, A. *Faraday Discuss.* **2008**, *140*, 233–244.
(41) Michaelides, A.; Ranea, V. A.; de Andres, P. L.; King, D. A. *Phys. Rev. Lett.* **2003**, *90*, 216102.
(42) Phatak, A. A.; Delgass, W. N.; Ribeiro, F. H.; Schneider, W. F. *J. Phys. Chem. C* **2009**, *113*, 7269–7276.

(43) Sebastiani, D.; Delle Site, L. *J. Chem. Theory Comput.* **2005**, *1*, 78−82.
(44) Lew, W.; Crowe, M. C.; Campbell, C. T.; Carrasco, J.; Michaelides, A. *J. Phys. Chem. C* **2011**, *115*, 23008−23012.
(45) Marsh, K. N. *Recommended Reference Materials for the Realization of Physicochemical Properties*; Oxford: Oxford, U.K., 1987.
(46) Rousseau, R.; De Renzi, V.; Mazzarello, R.; Marchetto, D.; Biagi, R.; Scandolo, S.; del Pennino, U. *J. Phys. Chem. B* **2006**, *110*, 10862−10872.
(47) Heimel, G.; Romaner, L.; Bredas, J. L.; Zojer, E. *Phys. Rev. Lett.* **2006**, *96*, 196806.
(48) Silva, J. L. F. D.; Stampfl, C.; Scheffler, M. *Phys. Rev. Lett.* **2003**, *90*, 066104.
(49) Michaelides, A.; Alavi, A.; King, D. A. *Phys. Rev. B* **2004**, *69*, 113404.
(50) Li, Z.; Zhang, Z.; Kim, Y. K.; Smith, R. S.; Netzer, F.; Kay, B. D.; Rousseau, R.; Dohnálek, Z. *J. Phys. Chem. C* **2011**, *115*, 5773−5783.
(51) Li, S.-C.; Li, Z.; Zhang, Z.; Kay, B. D.; Rousseau, R.; Dohnálek, Z. *J. Phys. Chem. C* **2011**, *116*, 908−916.
(52) Ogasawara, H.; Brena, B.; Nordlund, D.; Nyberg, M.; Pelmenschikov, A.; Pettersson, L. G. M.; Nilsson, A. *Phys. Rev. Lett.* **2002**, 89.
(53) Shang, C.; Liu, Z.-P. *J. Am. Chem. Soc.* **2011**, *133*, 9938−9947.
(54) Parr, R. G.; Yang, W. *Density Functional Theory of Atoms and Molecule*; Oxford University Press: New York, 1989.
(55) Rosenstock, H. M.; Draxl, K.; Steiner, B. W.; Herron, J. T. *J. Phys. Chem. Ref. Data* **1977**, *6*, 1.
(56) Parsons, G. H.; Rochester, C. H.; Wood, C. E. C. *J. Chem. Soc. B* **1971**, 533−536.
(57) Bader, R. *Atoms in Molecules: A Quantum Theory*; Oxford University Press: New York, 1990.
(58) Henkelman, G.; Arnaldsson, A.; Jonsson, H. *Comput. Mater. Sci.* **2006**, *36*, 354−360.
(59) Kirchner, B.; Stubbs, J.; Marx, D. *Phys. Rev. Lett.* **2002**, *89*, 215901.
(60) Dzingeleski, G. D.; Blotny, G.; Pollack, R. M. *J. Org. Chem.* **1990**, *55*, 1019−1023.
(61) Zhu, L.; Bozzelli, J. W. *J. Phys. Chem. A* **2003**, *107*, 3696−3703.